

Energy dependence of event shapes and of α_s at LEP 2

P. Abreu, W. Adam, T. Adye, P. Adzic, Z. Albrecht, T. Alderweireld, G.D. Alekseev, R. Alemany, T. Allmendinger, P.P. Allport, et al.

▶ **To cite this version:**

P. Abreu, W. Adam, T. Adye, P. Adzic, Z. Albrecht, et al.. Energy dependence of event shapes and of α_s at LEP 2. Physics Letters B, 1999, 456, pp.322-340. 10.1016/S0370-2693(99)00472-4 . in2p3-00002533

HAL Id: in2p3-00002533
https://hal.in2p3.fr/in2p3-00002533

Submitted on 23 Jun 1999

HAL is a multi-disciplinary open access archive for the deposit and dissemination of scientific research documents, whether they are published or not. The documents may come from teaching and research institutions in France or abroad, or from public or private research centers.

L'archive ouverte pluridisciplinaire **HAL**, est destinée au dépôt et à la diffusion de documents scientifiques de niveau recherche, publiés ou non, émanant des établissements d'enseignement et de recherche français ou étrangers, des laboratoires publics ou privés.

EUROPEAN ORGANIZATION FOR NUCLEAR RESEARCH

CERN–EP/99–44

16 March 1999

Energy Dependence of Event Shapes and of α_s at LEP 2

DELPHI Collaboration

Abstract

Infrared and collinear safe event shape distributions and their mean values are determined using the data taken at five different centre of mass energies above M_{Z} with the DELPHI detector at LEP. From the event shapes, the strong coupling α_s is extracted in $\mathcal{O}(\alpha_s^2)$, NLLA and a combined scheme using hadronisation corrections evaluated with fragmentation model generators as well as using an analytical power ansatz. Comparing these measurements to those obtained at M_{Z}, the energy dependence (running) of α_s is accessible. The logarithmic energy slope of the inverse strong coupling is measured to be

$$\frac{d\alpha_s^{-1}}{d\log(E_{\mathrm{cm}})} = 1.39 \pm 0.34(stat) \pm 0.17(syst) \quad ,$$

in good agreement with the QCD expectation of 1.27.

(Accepted by Physics Letters B)

P.Abreu[21], W.Adam[50], T.Adye[36], P.Adzic[11], Z.Albrecht[17], T.Alderweireld[2], G.D.Alekseev[16], R.Alemany[49], T.Allmendinger[17], P.P.Allport[22], S.Almehed[24], U.Amaldi[9], N.Amapane[45], S.Amato[47], E.G.Anassontzis[3], P.Andersson[44], A.Andreazza[9], S.Andringa[21], P.Antilogus[25], W-D.Apel[17], Y.Arnoud[9], B.Åsman[44], J-E.Augustin[25], A.Augustinus[9], P.Baillon[9], P.Bambade[19], F.Barao[21], G.Barbiellini[46], R.Barbier[25], D.Y.Bardin[16], G.Barker[17], A.Baroncelli[38], M.Battaglia[15], M.Baubillier[23], K-H.Becks[52], M.Begalli[6], A.Behrmann[52], P.Beilliere[8], Yu.Belokopytov[9,53], K.Belous[42], N.C.Benekos[31], A.C.Benvenuti[5], C.Berat[14], M.Berggren[25], D.Bertini[25], D.Bertrand[2], M.Besancon[39], F.Bianchi[45], M.Bigi[45], M.S.Bilenky[16], M-A.Bizouard[19], D.Bloch[10], H.M.Blom[30], M.Bonesini[27], W.Bonivento[27], M.Boonekamp[39], P.S.L.Booth[22], A.W.Borgland[4], G.Borisov[19], C.Bosio[41], O.Botner[48], E.Boudinov[30], B.Bouquet[19], C.Bourdarios[19], T.J.V.Bowcock[22], I.Boyko[16], I.Bozovic[11], M.Bozzo[13], P.Branchini[38], T.Brenke[52], R.A.Brenner[48], P.Bruckman[18], J-M.Brunet[8], L.Bugge[32], T.Buran[32], T.Burgsmueller[52], B.Buschbeck[50], P.Buschmann[52], S.Cabrera[49], M.Caccia[27], M.Calvi[27], T.Camporesi[9], V.Canale[37], F.Carena[9], L.Carroll[22], C.Caso[13], M.V.Castillo Gimenez[49], A.Cattai[9], F.R.Cavallo[5], V.Chabaud[9], M.Chapkin[42], Ph.Charpentier[9], L.Chaussard[25], P.Checchia[35], G.A.Chelkov[16], R.Chierici[45], P.Chliapnikov[42], P.Chochula[7], V.Chorowicz[25], J.Chudoba[29], K.Cieslik[18], P.Collins[9], R.Contri[13], E.Cortina[49], G.Cosme[19], F.Cossutti[9], J-H.Cowell[22], H.B.Crawley[1], D.Crennell[36], S.Crepe[14], G.Crosetti[13], J.Cuevas Maestro[33], S.Czellar[15], M.Davenport[9], W.Da Silva[23], A.Deghorain[2], G.Della Ricca[46], P.Delpierre[26], N.Demaria[9], A.De Angelis[9], W.De Boer[17], C.De Clercq[2], B.De Lotto[46], A.De Min[35], L.De Paula[47], H.Dijkstra[9], L.Di Ciaccio[37,9], J.Dolbeau[8], K.Doroba[51], M.Dracos[10], J.Drees[52], M.Dris[31], A.Duperrin[25], J-D.Durand[9], G.Eigen[4], T.Ekelof[48], G.Ekspong[44], M.Ellert[48], M.Elsing[9], J-P.Engel[10], B.Erzen[43], M.Espirito Santo[21], E.Falk[24], G.Fanourakis[11], D.Fassouliotis[11], J.Fayot[23], M.Feindt[17], A.Fenyuk[42], P.Ferrari[27], A.Ferrer[49], E.Ferrer-Ribas[19], F.Ferro[13], S.Fichet[23], A.Firestone[1], U.Flagmeyer[52], H.Foeth[9], E.Fokitis[31], F.Fontanelli[13], B.Franek[36], A.G.Frodesen[4], R.Fruhwirth[50], F.Fulda-Quenzer[19], J.Fuster[49], A.Galloni[22], D.Gamba[45], S.Gamblin[19], M.Gandelman[47], C.Garcia[49], C.Gaspar[9], M.Gaspar[47], U.Gasparini[35], Ph.Gavillet[9], E.N.Gazis[31], D.Gele[10], N.Ghodbane[25], I.Gil[49], F.Glege[52], R.Gokieli[9,51], B.Golob[43], G.Gomez-Ceballos[40], P.Goncalves[21], I.Gonzalez Caballero[40], G.Gopal[36], L.Gorn[1,54], M.Gorski[51], Yu.Gouz[42], V.Gracco[13], J.Grahl[1], E.Graziani[38], C.Green[22], H-J.Grimm[17], P.Gris[39], G.Grosdidier[19], K.Grzelak[51], M.Gunther[48], J.Guy[36], F.Hahn[9], S.Hahn[52], S.Haider[9], A.Hallgren[48], K.Hamacher[52], J.Hansen[32], F.J.Harris[34], V.Hedberg[24], S.Heising[17], J.J.Hernandez[49], P.Herquet[2], H.Herr[9], T.L.Hessing[34], J.-M.Heuser[52], E.Higon[49], S-O.Holmgren[44], P.J.Holt[34], S.Hoorelbeke[2], M.Houlden[22], J.Hrubec[50], K.Huet[2], G.J.Hughes[22], K.Hultqvist[44], J.N.Jackson[22], R.Jacobsson[9], P.Jalocha[9], R.Janik[7], Ch.Jarlskog[24], G.Jarlskog[24], P.Jarry[39], B.Jean-Marie[19], E.K.Johansson[44], P.Jonsson[25], C.Joram[9], P.Juillot[10], F.Kapusta[23], K.Karafasoulis[11], S.Katsanevas[25], E.C.Katsoufis[31], R.Keranen[17], B.P.Kersevan[43], B.A.Khomenko[16], N.N.Khovanski[16], A.Kiiskinen[15], B.King[22], A.Kinvig[22], N.J.Kjaer[30], O.Klapp[52], H.Klein[9], P.Kluit[30], P.Kokkinias[11], M.Koratzinos[9], V.Kostioukhine[42], C.Kourkoumelis[3], O.Kouznetsov[39], M.Krammer[50], E.Kriznic[43], P.Krstic[11], Z.Krumstein[16], P.Kubinec[7], J.Kurowska[51], K.Kurvinen[15], J.W.Lamsa[1], D.W.Lane[1], P.Langefeld[52], V.Lapin[42], J-P.Laugier[39], R.Lauhakangas[15], G.Leder[50], F.Ledroit[14], V.Lefebure[2], L.Leinonen[44], A.Leisos[11], R.Leitner[29], J.Lemonne[2], G.Lenzen[52], V.Lepeltier[19], T.Lesiak[18], M.Lethuillier[39], J.Libby[34], D.Liko[9], A.Lipniacka[44], I.Lippi[35], B.Loerstad[24], J.G.Loken[34], J.H.Lopes[47], J.M.Lopez[40], R.Lopez-Fernandez[14], D.Loukas[11], P.Lutz[39], L.Lyons[34], J.MacNaughton[50], J.R.Mahon[6], A.Maio[21], A.Malek[52], T.G.M.Malmgren[44], S.Maltezos[31], V.Malychev[16], F.Mandl[50], J.Marco[40], R.Marco[40], B.Marechal[47], M.Margoni[35], J-C.Marin[9], C.Mariotti[9], A.Markou[11], C.Martinez-Rivero[19], F.Martinez-Vidal[49], S.Marti i Garcia[9], J.Masik[12], N.Mastroyiannopoulos[11], F.Matorras[40], C.Matteuzzi[27], G.Matthiae[37], F.Mazzucato[35], M.Mazzucato[35], M.Mc Cubbin[22], R.Mc Kay[1], R.Mc Nulty[22], G.Mc Pherson[22], C.Meroni[27], W.T.Meyer[1], E.Migliore[45], L.Mirabito[25], W.A.Mitaroff[50], U.Mjoernmark[24], T.Moa[44], M.Moch[17], R.Moeller[28], K.Moenig[9], M.R.Monge[13], X.Moreau[23], P.Morettini[13], G.Morton[34], U.Mueller[52], K.Muenich[52], M.Mulders[30], C.Mulet-Marquis[14], R.Muresan[24], W.J.Murray[36], B.Muryn[14,18], G.Myatt[34], T.Myklebust[32], F.Naraghi[14], M.Nassiakou[11], F.L.Navarria[5], S.Navas[49], K.Nawrocki[51], P.Negri[27], S.Nemecek[12], N.Neufeld[9], N.Neumeister[50], R.Nicolaidou[39], B.S.Nielsen[28], M.Nikolenko[10,16], V.Nomokonov[15], A.Normand[22], A.Nygren[24], V.Obraztsov[42], A.G.Olshevski[16], A.Onofre[21], R.Orava[15], G.Orazi[10], K.Osterberg[15], A.Ouraou[39], M.Paganoni[27], S.Paiano[5], R.Pain[23], R.Paiva[21], J.Palacios[34], H.Palka[18], Th.D.Papadopoulou[31,9], K.Papageorgiou[11], L.Pape[9], C.Parkes[9], F.Parodi[13], U.Parzefall[22], A.Passeri[38], O.Passon[52], M.Pegoraro[35], L.Peralta[21], M.Pernicka[50], A.Perrotta[5], C.Petridou[46], A.Petrolini[13], H.T.Phillips[36], F.Pierre[39], M.Pimenta[21], E.Piotto[27], T.Podobnik[43], M.E.Pol[6], G.Polok[18], P.Poropat[46], V.Pozdniakov[16], P.Privitera[37], N.Pukhaeva[16], A.Pullia[27], D.Radojicic[34], S.Ragazzi[27], H.Rahmani[31], P.N.Ratoff[20], A.L.Read[32], P.Rebecchi[9], N.G.Redaelli[27], M.Regler[50], D.Reid[30], R.Reinhardt[52], P.B.Renton[34], L.K.Resvanis[3], F.Richard[19], J.Ridky[12], G.Rinaudo[45], O.Rohne[32], A.Romero[45], P.Ronchese[35], E.I.Rosenberg[1], P.Rosinsky[7], P.Roudeau[19], T.Rovelli[5], Ch.Royon[39], V.Ruhlmann-Kleider[39], A.Ruiz[40], H.Saarikko[15], Y.Sacquin[39], A.Sadovsky[16], G.Sajot[14], J.Salt[49], D.Sampsonidis[11], M.Sannino[13], H.Schneider[17], Ph.Schwemling[23], B.Schwering[52], U.Schwickerath[17], M.A.E.Schyns[52], F.Scuri[46], P.Seager[20], Y.Sedykh[16], A.M.Segar[34], R.Sekulin[36], R.C.Shellard[6], A.Sheridan[22], M.Siebel[52], L.Simard[39], F.Simonetto[35], A.N.Sisakian[16], G.Smadja[25], N.Smirnov[42], O.Smirnova[24], G.R.Smith[36], A.Sopczak[17], R.Sosnowski[51], T.Spassov[21], E.Spiriti[38], P.Sponholz[52], S.Squarcia[13], C.Stanescu[38], S.Stanic[43], K.Stevenson[34], A.Stocchi[19], R.Strub[10], B.Stugu[4], M.Szczekowski[51], M.Szeptycka[51], T.Tabarelli[27], F.Tegenfeldt[48], F.Terranova[27], J.Thomas[34], J.Timmermans[30], N.Tinti[5], L.G.Tkatchev[16], S.Todorova[10], A.Tomaradze[2], B.Tome[21], A.Tonazzo[9],

L.Tortora[38], G.Transtromer[24], D.Treille[9], G.Tristram[8], M.Trochimczuk[51], C.Troncon[27], A.Tsirou[9], M-L.Turluer[39], I.A.Tyapkin[16], S.Tzamarias[11], O.Ullaland[9], V.Uvarov[42], G.Valenti[5], E.Vallazza[46], C.Vander Velde[2], G.W.Van Apeldoorn[30], P.Van Dam[30], W.K.Van Doninck[2], J.Van Eldik[30], A.Van Lysebetten[2], I.Van Vulpen[30], N.Vassilopoulos[34], G.Vegni[27], L.Ventura[35], W.Venus[36,9], F.Verbeure[2], M.Verlato[35], L.S.Vertogradov[16], V.Verzi[37], D.Vilanova[39], L.Vitale[46], E.Vlasov[42], A.S.Vodopyanov[16], C.Vollmer[17], G.Voulgaris[3], V.Vrba[12], H.Wahlen[52], C.Walck[44], C.Weiser[17], D.Wicke[52], J.H.Wickens[2], G.R.Wilkinson[9], M.Winter[10], M.Witek[18], G.Wolf[9], J.Yi[1], O.Yushchenko[42], A.Zaitsev[42], A.Zalewska[18], P.Zalewski[51], D.Zavrtanik[43], E.Zevgolatakos[11], N.I.Zimin[16,24], G.C.Zucchelli[44], G.Zumerle[35]

[1]Department of Physics and Astronomy, Iowa State University, Ames IA 50011-3160, USA
[2]Physics Department, Univ. Instelling Antwerpen, Universiteitsplein 1, BE-2610 Wilrijk, Belgium
and IIHE, ULB-VUB, Pleinlaan 2, BE-1050 Brussels, Belgium
and Faculté des Sciences, Univ. de l'Etat Mons, Av. Maistriau 19, BE-7000 Mons, Belgium
[3]Physics Laboratory, University of Athens, Solonos Str. 104, GR-10680 Athens, Greece
[4]Department of Physics, University of Bergen, Allégaten 55, NO-5007 Bergen, Norway
[5]Dipartimento di Fisica, Università di Bologna and INFN, Via Irnerio 46, IT-40126 Bologna, Italy
[6]Centro Brasileiro de Pesquisas Físicas, rua Xavier Sigaud 150, BR-22290 Rio de Janeiro, Brazil
and Depto. de Física, Pont. Univ. Católica, C.P. 38071 BR-22453 Rio de Janeiro, Brazil
and Inst. de Física, Univ. Estadual do Rio de Janeiro, rua São Francisco Xavier 524, Rio de Janeiro, Brazil
[7]Comenius University, Faculty of Mathematics and Physics, Mlynska Dolina, SK-84215 Bratislava, Slovakia
[8]Collège de France, Lab. de Physique Corpusculaire, IN2P3-CNRS, FR-75231 Paris Cedex 05, France
[9]CERN, CH-1211 Geneva 23, Switzerland
[10]Institut de Recherches Subatomiques, IN2P3 - CNRS/ULP - BP20, FR-67037 Strasbourg Cedex, France
[11]Institute of Nuclear Physics, N.C.S.R. Demokritos, P.O. Box 60228, GR-15310 Athens, Greece
[12]FZU, Inst. of Phys. of the C.A.S. High Energy Physics Division, Na Slovance 2, CZ-180 40, Praha 8, Czech Republic
[13]Dipartimento di Fisica, Università di Genova and INFN, Via Dodecaneso 33, IT-16146 Genova, Italy
[14]Institut des Sciences Nucléaires, IN2P3-CNRS, Université de Grenoble 1, FR-38026 Grenoble Cedex, France
[15]Helsinki Institute of Physics, HIP, P.O. Box 9, FI-00014 Helsinki, Finland
[16]Joint Institute for Nuclear Research, Dubna, Head Post Office, P.O. Box 79, RU-101 000 Moscow, Russian Federation
[17]Institut für Experimentelle Kernphysik, Universität Karlsruhe, Postfach 6980, DE-76128 Karlsruhe, Germany
[18]Institute of Nuclear Physics and University of Mining and Metalurgy, Ul. Kawiory 26a, PL-30055 Krakow, Poland
[19]Université de Paris-Sud, Lab. de l'Accélérateur Linéaire, IN2P3-CNRS, Bât. 200, FR-91405 Orsay Cedex, France
[20]School of Physics and Chemistry, University of Lancaster, Lancaster LA1 4YB, UK
[21]LIP, IST, FCUL - Av. Elias Garcia, 14-1^o, PT-1000 Lisboa Codex, Portugal
[22]Department of Physics, University of Liverpool, P.O. Box 147, Liverpool L69 3BX, UK
[23]LPNHE, IN2P3-CNRS, Univ. Paris VI et VII, Tour 33 (RdC), 4 place Jussieu, FR-75252 Paris Cedex 05, France
[24]Department of Physics, University of Lund, Sölvegatan 14, SE-223 63 Lund, Sweden
[25]Université Claude Bernard de Lyon, IPNL, IN2P3-CNRS, FR-69622 Villeurbanne Cedex, France
[26]Univ. d'Aix - Marseille II - CPP, IN2P3-CNRS, FR-13288 Marseille Cedex 09, France
[27]Dipartimento di Fisica, Università di Milano and INFN, Via Celoria 16, IT-20133 Milan, Italy
[28]Niels Bohr Institute, Blegdamsvej 17, DK-2100 Copenhagen Ø, Denmark
[29]NC, Nuclear Centre of MFF, Charles University, Areal MFF, V Holesovickach 2, CZ-180 00, Praha 8, Czech Republic
[30]NIKHEF, Postbus 41882, NL-1009 DB Amsterdam, The Netherlands
[31]National Technical University, Physics Department, Zografou Campus, GR-15773 Athens, Greece
[32]Physics Department, University of Oslo, Blindern, NO-1000 Oslo 3, Norway
[33]Dpto. Fisica, Univ. Oviedo, Avda. Calvo Sotelo s/n, ES-33007 Oviedo, Spain
[34]Department of Physics, University of Oxford, Keble Road, Oxford OX1 3RH, UK
[35]Dipartimento di Fisica, Università di Padova and INFN, Via Marzolo 8, IT-35131 Padua, Italy
[36]Rutherford Appleton Laboratory, Chilton, Didcot OX11 OQX, UK
[37]Dipartimento di Fisica, Università di Roma II and INFN, Tor Vergata, IT-00173 Rome, Italy
[38]Dipartimento di Fisica, Università di Roma III and INFN, Via della Vasca Navale 84, IT-00146 Rome, Italy
[39]DAPNIA/Service de Physique des Particules, CEA-Saclay, FR-91191 Gif-sur-Yvette Cedex, France
[40]Instituto de Fisica de Cantabria (CSIC-UC), Avda. los Castros s/n, ES-39006 Santander, Spain
[41]Dipartimento di Fisica, Università degli Studi di Roma La Sapienza, Piazzale Aldo Moro 2, IT-00185 Rome, Italy
[42]Inst. for High Energy Physics, Serpukov P.O. Box 35, Protvino, (Moscow Region), Russian Federation
[43]J. Stefan Institute, Jamova 39, SI-1000 Ljubljana, Slovenia and Laboratory for Astroparticle Physics,
Nova Gorica Polytechnic, Kostanjeviska 16a, SI-5000 Nova Gorica, Slovenia,
and Department of Physics, University of Ljubljana, SI-1000 Ljubljana, Slovenia
[44]Fysikum, Stockholm University, Box 6730, SE-113 85 Stockholm, Sweden
[45]Dipartimento di Fisica Sperimentale, Università di Torino and INFN, Via P. Giuria 1, IT-10125 Turin, Italy
[46]Dipartimento di Fisica, Università di Trieste and INFN, Via A. Valerio 2, IT-34127 Trieste, Italy
and Istituto di Fisica, Università di Udine, IT-33100 Udine, Italy
[47]Univ. Federal do Rio de Janeiro, C.P. 68528 Cidade Univ., Ilha do Fundão BR-21945-970 Rio de Janeiro, Brazil
[48]Department of Radiation Sciences, University of Uppsala, P.O. Box 535, SE-751 21 Uppsala, Sweden
[49]IFIC, Valencia-CSIC, and D.F.A.M.N., U. de Valencia, Avda. Dr. Moliner 50, ES-46100 Burjassot (Valencia), Spain
[50]Institut für Hochenergiephysik, Österr. Akad. d. Wissensch., Nikolsdorfergasse 18, AT-1050 Vienna, Austria
[51]Inst. Nuclear Studies and University of Warsaw, Ul. Hoza 69, PL-00681 Warsaw, Poland
[52]Fachbereich Physik, University of Wuppertal, Postfach 100 127, DE-42097 Wuppertal, Germany
[53]On leave of absence from IHEP Serpukhov
[54]Now at University of Florida

1 Introduction

From 1995 to 1997 LEP operated at five different centre of mass energies between 130 GeV and 183 GeV. The statistics of hadronic events collected at these energies, though small compared to the statistics gathered near the Z resonance, is sufficient for the measurement of event shape distributions and for a determination of the strong coupling α_s. To obtain the running of α_s the data taken at 91.2 GeV in 1993–95 were reanalysed using cuts, binnings and fit ranges coherent with the high energy data analysis.

This paper summarises event shape distributions and their moments measured using DELPHI [?,?]. For each energy, α_s is measured using various techniques: fits to shape distributions in second order perturbation theory[?], in the next-to-leading-log approximation (NLLA) [?,?], and in a combined $\mathcal{O}(\alpha_s^2)$+NLLA scheme [?] are performed in connection with Monte Carlo based hadronisation models. Alternatively, fits to the energy dependence of mean values are used to fix the only free parameter in the power correction formula [?,?,?,?], allowing one to obtain α_s independent of the above mentioned models. Finally, the resulting energy dependence of α_s, as determined with the different methods, is compared to the QCD expectation and an extended theory including gluinos.

In section 2 the selection of hadronic events, the reconstruction of the centre of mass energy, the correction procedures applied to the data, and for energies above the WW threshold the suppression of W^+W^- events are briefly discussed. Section 3 presents event shapes and jet rates and the comparison of the data with predictions from $q\bar{q}$-based hadronic generators. In section 4, measurements of α_s using the various techniques and the running of α_s, as determined with the different methods, are presented.

2 Selection and correction of hadronic data

The analysis is based on data at six different centre of mass energies between 91.2 GeV and 183 GeV. The results for 91.2 GeV are obtained using 1993 to 1995 data. The data taken at 130 GeV and 136 GeV in the years 1995 and 1997 are averaged and given as results at $E_{\mathrm{cm}} = 133$ GeV, their average centre of mass energy. The integrated luminosities collected at the higher energies are given in Table 1.

DELPHI is a hermetic detector with a solenoidal magnetic field of 1.2 T. The tracking detectors, situated in front of the electromagnetic calorimeters are a silicon micro-vertex

E_{cm}	133 GeV	161 GeV	172 GeV	183 GeV
$\mathcal{L}$	11.9 pb^{-1}	10.1 pb^{-1}	10.0 pb^{-1}	54 pb^{-1}
$\sigma_{q\bar{q}}$	292 pb	147 pb	121.0 pb	100.3 pb
$\sigma_{q\bar{q}\ (\sqrt{s'}>0.85\sqrt{s})}$	74 pb	35 pb	29 pb	24.5 pb
σ_{WW}	—	3.3 pb	12.1 pb	15.4 pb
Number of events	846	359	289	1338

Table 1: Total cross sections $\sigma_{q\bar{q}}$ and σ_{WW} as used in the simulation, high energy cross sections $\sigma_{q\bar{q}\ (\sqrt{s'}>0.85\sqrt{s})}$ as predicted by ZFITTER 5.12 [?], integrated luminosities $\mathcal{L}$, and finally selected (non-radiative) hadronic events for the various energies.

Track selection	$0.4\,\mathrm{GeV} \leq p \leq 100\,\mathrm{GeV}$
	$\Delta p/p \leq 1.0$
	measured track length ≥ 30 cm
	distance to I.P in $r\phi$ plane ≤ 4 cm
	distance to I.P. in $z \leq 10$ cm

Table 2: Selection of tracks. p is the momentum, Δp its error, r the radial distance to the beam-axis, z the distance to the beam interaction point (I.P.) along the beam-axis, ϕ the azimuthal angle. The first two cuts apply to charged and neutral particles, while the others apply to charged particles only.

	Observable	Central cut	Cut variations	
Event selection	N_{ch}	≥ 7	≥ 6	≥ 8
	θ_{Thrust}	$[25°, 155°]$	$[20°, 160°]$	$[30°, 150°]$
	E_{tot}	$\geq 0.50 E_{\mathrm{cm}}$	$\geq 0.45 E_{\mathrm{cm}}$	$\geq 0.55 E_{\mathrm{cm}}$
ISR Rejection	$\sqrt{s'_{\mathrm{rec}}}$	$\geq 90\% E_{\mathrm{cm}}$	$\geq 80\% E_{\mathrm{cm}}$	
WW/ZZ Rejection ($E_{\mathrm{cm}} \geq 161\,\mathrm{GeV}$)	N_{ch}	≤ 42	$\leq \infty$	
	B_{min}	≤ 0.08	≤ 0.10	

Table 3: Selection of events. N_{charged} is the number of charged particles, θ_{Thrust} the polar angle of the thrust axis with respect to the beam, E_{tot} the total energy carried by all particles, $\sqrt{s'_{\mathrm{rec}}}$ the reconstructed centre of mass energy, $E_{\mathrm{cm}} = \sqrt{s}$ the nominal centre of mass energy, and B_{min} is the minimal jet broadening.

detector VD, a combined jet/proportional chamber inner detector ID, a time projection chamber TPC as the major tracking device, and the streamer tube detector OD in the barrel region. The forward region is covered by silicon mini-strip and pixel detectors (VFT) and by the drift chamber detectors FCA and FCB.

The electromagnetic calorimeters are the high density projection chamber HPC in the barrel, and the lead-glass calorimeter FEMC in the forward region. Detailed information about the design and performance of DELPHI can be found in [**?**,**?**].

In order to select well measured charged particle tracks, the cuts given in Table 2 have been applied. The cuts in Table 3 are used to select $e^+e^- \to \mathrm{Z}/\gamma \to q\bar{q}$ events and to suppress background processes such as two-photon interactions, beam-gas and beam-wall interactions, leptonic final states, and, for the LEP2 analysis, initial state radiation (ISR) and WW pair production (for energies above the WW threshold).

At energies above 91.2 GeV, the high cross section of the Z resonance peak raises the possibility of hard ISR allowing the creation of a nearly on-shell Z boson. These "radiative return events" constitute a large fraction of all hadronic events. The initial state photons are typically aligned along the beam direction and are rarely identified inside the detector. In order to evaluate the effective hadronic centre of mass energy of an event, considering ISR, an algorithm called SPRIME+ is used [**?**]. SPRIME+ is based on a fit imposing four-momentum conservation to measured jet four-momenta (including estimates of their errors). Several assumptions about the event topology are tested. The

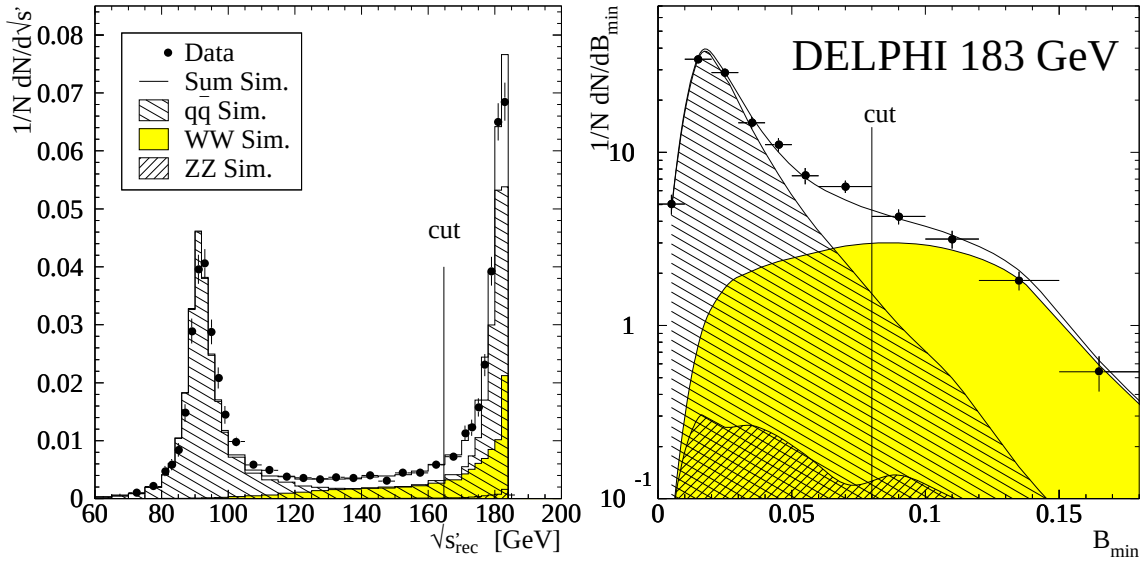


Figure 1: Left: reconstructed centre of mass energy (data with $E_{\rm cm} = 183\,\text{GeV}$). Right: discriminant variables $B_{\rm min}$ for $q\bar{q}$, WW and ZZ events, $E_{\rm cm} = 183\,\text{GeV}$. In both plots the simulations are based on PYTHIA [?] and DELSIM [?]. Data are shown before WW cuts and without WW subtraction, in the left plot also without ISR cut.

decision is taken according to the χ^2 obtained from the constrained fits with different topologies.

Figure 1(left) shows the spectra of the calculated energies for simulated and measured events passing general event cuts for the 183 GeV data.The agreement between data and simulation is very good for the high energies relevant to this analysis, while the peak around $M_{\rm Z}$ appears to be slightly shifted in the simulation. A cut on the reconstructed centre of mass energy $\sqrt{s'_{\rm rec}} \geq 90\% E_{\rm cm}$ is applied to discard radiative return events (see Table 3). Simulation shows that this cut keeps more than 96% of the events without ISR ($\sqrt{s} - \sqrt{s'} < 0.1\,\text{GeV}$), giving a contamination with events having $\sqrt{s} - \sqrt{s'} > 10\,\text{GeV}$ of less than 15%.

Two photon events are strongly suppressed by the cuts. Leptonic background is found to be negligible in this analysis.

Since the topological signatures of QCD four jet events and hadronic WW events (and other four quark backgrounds) are similar, no highly efficient separation of the two classes of events is possible. Furthermore any WW rejection implies a severe bias to the shape distributions of QCD events, which needs to be corrected with simulation. By applying a cut on an observable calculated from the narrow event hemisphere only, the bias to event shape observables mainly sensitive to the wide event hemisphere is reduced. To separate $q\bar{q}$ from WW events, the shape $B_{\rm min}$ (as defined in [?]) is chosen. The discrimination due to $B_{\rm min}$ is demonstrated in Figure 1(right) for the 183 GeV data, the actual cut applied to data with $E_{\rm cm} \geq 161\,\text{GeV}$ is $B_{\rm min} \leq 0.08$.

The remaining WW contribution is estimated by Monte Carlo generators and subtracted from the measurement. The simulations are normalised using the cross sections given in Table 1. The quoted $\sigma_{\rm WW}$ values correspond to a W mass of 80.35 GeV. An alternative multiplicative correction with a fixed signal to background ratio, would lead to smaller statistical errors, but implies a strong bias towards the $q\bar{q}$-simulation.

The remaining detector and cut effects are unfolded with simulation. The influence of detector effects was studied by passing generated events (JETSET/PYTHIA [?] using the DELPHI tuning described in [?]) through a full detector simulation (DELSIM [?]). These Monte Carlo events are processed with the reconstruction program and selection cuts as are the real data. In order to correct for cuts, detector, and ISR effects a bin by bin acceptance correction C, obtained from $e^+e^- \to \mathrm{Z}/\gamma \to q\bar{q}$ simulation, is applied to the data:

$$C_i = C_{i,\mathrm{QCD}} \cdot C_{i,\mathrm{WW}} = \frac{h(f_i)_{\mathrm{gen,noISR}}}{h(f_i)_{\mathrm{qcdacc}}} \cdot \frac{h(f_i)_{\mathrm{qcdacc}}}{h(f_i)_{\mathrm{acc}}} \tag{1}$$

where $h(f_i)_{\mathrm{gen,noISR}}$ represents bin i of the shape distribution f generated with the tuned generator. The subscript noISR indicates that only events without relevant ISR ($\sqrt{s} - \sqrt{s'} < 0.1\,\mathrm{GeV}$) enter the distribution. $h(f_i)_{\ldots\mathrm{acc}}$ represents the accepted distribution f as obtained with the full detector simulation. For $h(f_i)_{\mathrm{qcdacc}}$ all but WW cuts are applied, for $h(f_i)_{\mathrm{acc}}$ also the WW cuts are applied. At centre-of-mass energies below 161 GeV the factor C_{WW} equals one.

3 Event shape observables

Selected event shape distributions are shown in Figures 2–5. Figures 2, 3 and 5 show the results from 183 GeV centre of mass energy, while Figure 4 gives the energy dependence of the observable Thrust as an example. The numerical results for these and further observables have been given to the Durham-RAL database [?]. The exact definitions of the observables used are comprehensively collected in Appendix A of [?].

The data in Figures 2–5 are corrected to be comparable with pure $e^+e^- \to \mathrm{Z}/\gamma \to q\bar{q}$ simulation of charged and neutral hadron production. The line in the central part of each figure shows the corresponding JETSET/PYTHIA PS simulation. The amount of WW-background that was subtracted to obtain the final data points is given as a shaded area. In the lower insets the efficiency times the purity of the WW specific cuts is shown. The acceptance corrections are plotted in the upper inset, split into the detector/cut corrections C_{QCD}, C_{WW} as described in section 2 and the WW subtraction effect. The plots show a good agreement between the data and Monte Carlo models.

Table 7 gives the moments of some QCD relevant shape variables. The means and moments are calculated by integrating the fully corrected (binned) shape distributions. In order to correct for the error due to binning, a correction factor calculated as the ratio of the exact simulation result over the binned simulation result is applied. The uncertainty due to this correction is accounted for by adding 10% of this binning correction as well as 10% of the change due to the correction factors C_{QCD} and C_{WW} to the moments systematic errors. In addition, contributions to the systematic error were included from changes arising from varying the ISR, WW and event cuts (as indicated in Table 3) as well as changing the assumed WW cross section by 5% (10% for 161 GeV). Finally the effect of replacing JETSET/PYTHIA by HERWIG 5.8d [?] as basis for the detector simulation DELSIM was investigated. Though HERWIG implements a more complete description of ISR, the resulting systematic error contribution is small.

For some observables the spread of the results obtained in three individual years of Z-peak data taking exceeds the estimated systematic error. In this case this spread is taken as systematic error.

When dealing with small samples of data, systematic errors from cut variations can be overestimated because of purely statistical fluctuations [?]. To check the reliability of

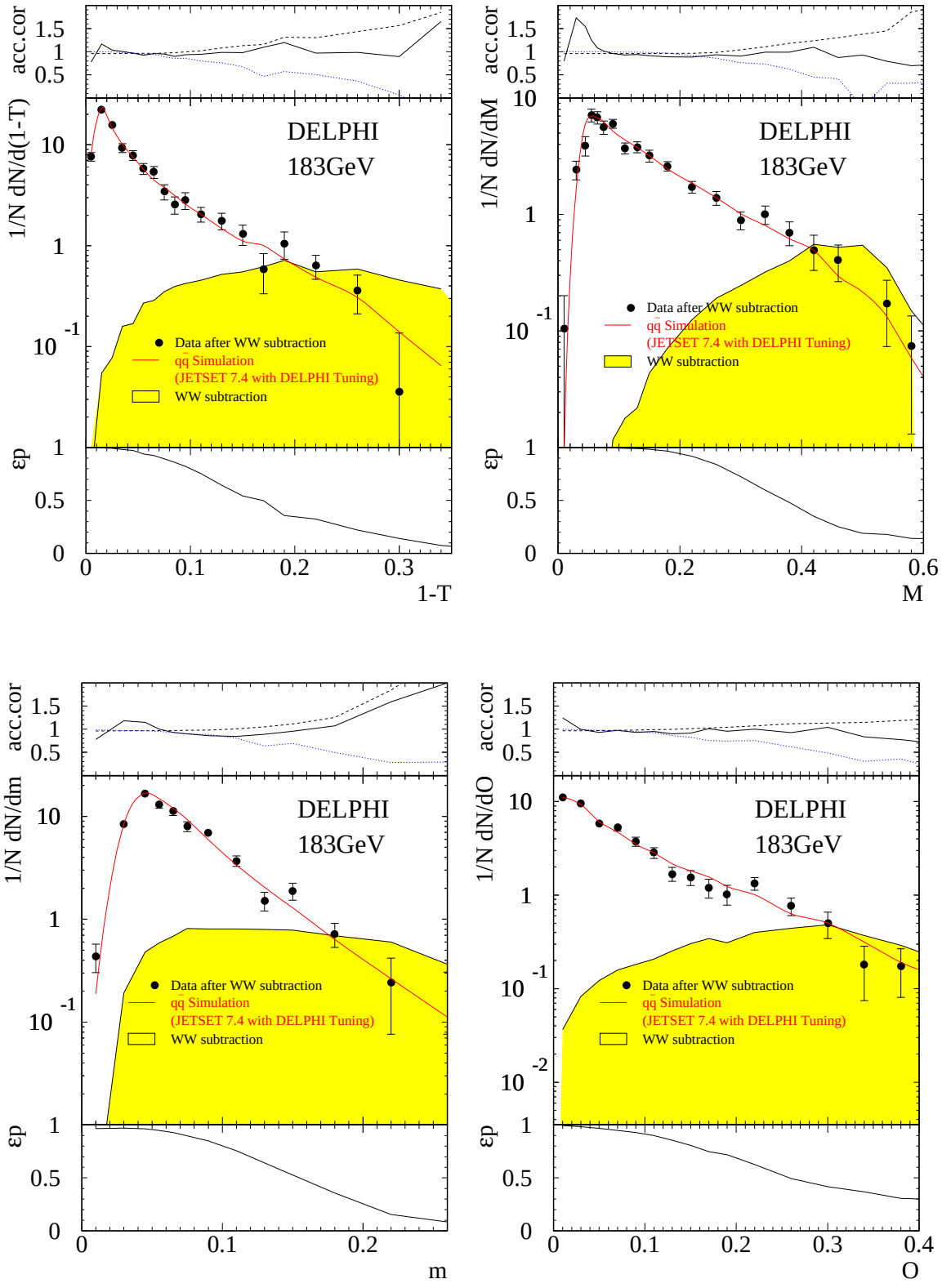


Figure 2: Event shape distributions of Thrust (T), Major (M), Minor (m), and Oblateness (O) at 183 GeV. The upper inset shows acceptance corrections: the QCD corrections C_{QCD} as continuous line, the QCD correction due to WW-cuts C_{WW} as dashed line and the ratio of data after and before WW subtraction as dotted line. The middle part shows data, simulation and WW background. The lower part shows the efficiency times purity of the applied WW-cuts.

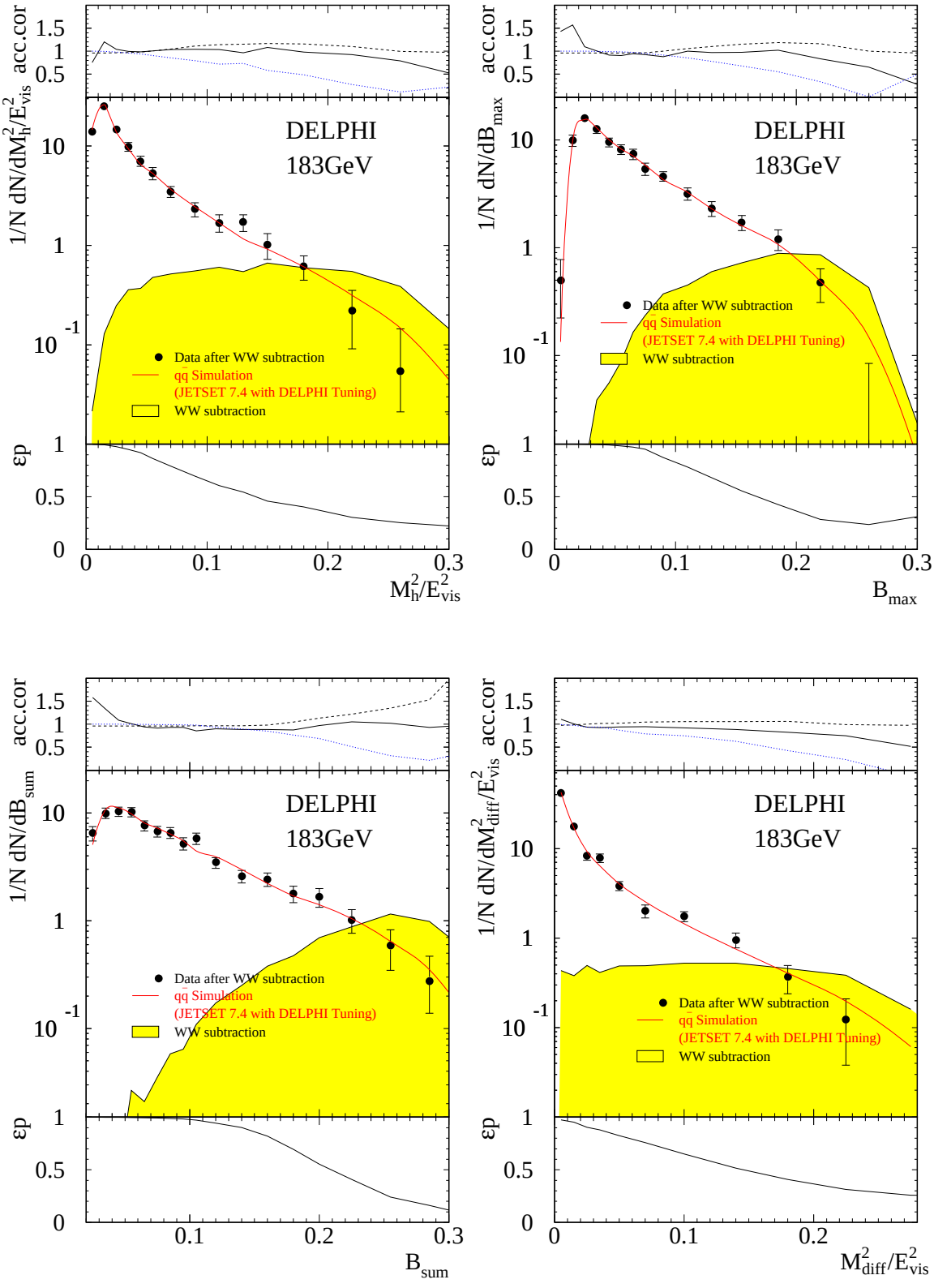


Figure 3: Event shape distributions of Heavy Jetmass ($M_{\mathrm{h}}^2/E_{\mathrm{vis}}^2$), Wide Jetbroadening ($B_{\mathrm{max}}$), Total Jetbroadening ($B_{\mathrm{sum}}$), and Jetmass Difference ($M_{\mathrm{diff}}^2/E_{\mathrm{vis}}^2$) at 183 GeV. The upper inset shows acceptance corrections: the QCD corrections C_{QCD} as continuous line, the QCD correction due to WW-cuts C_{WW} as dashed line and the ratio of data after and before WW subtraction as dotted line. The middle part shows data, simulation and WW background. The lower part shows the efficiency times purity of the applied WW-cuts.

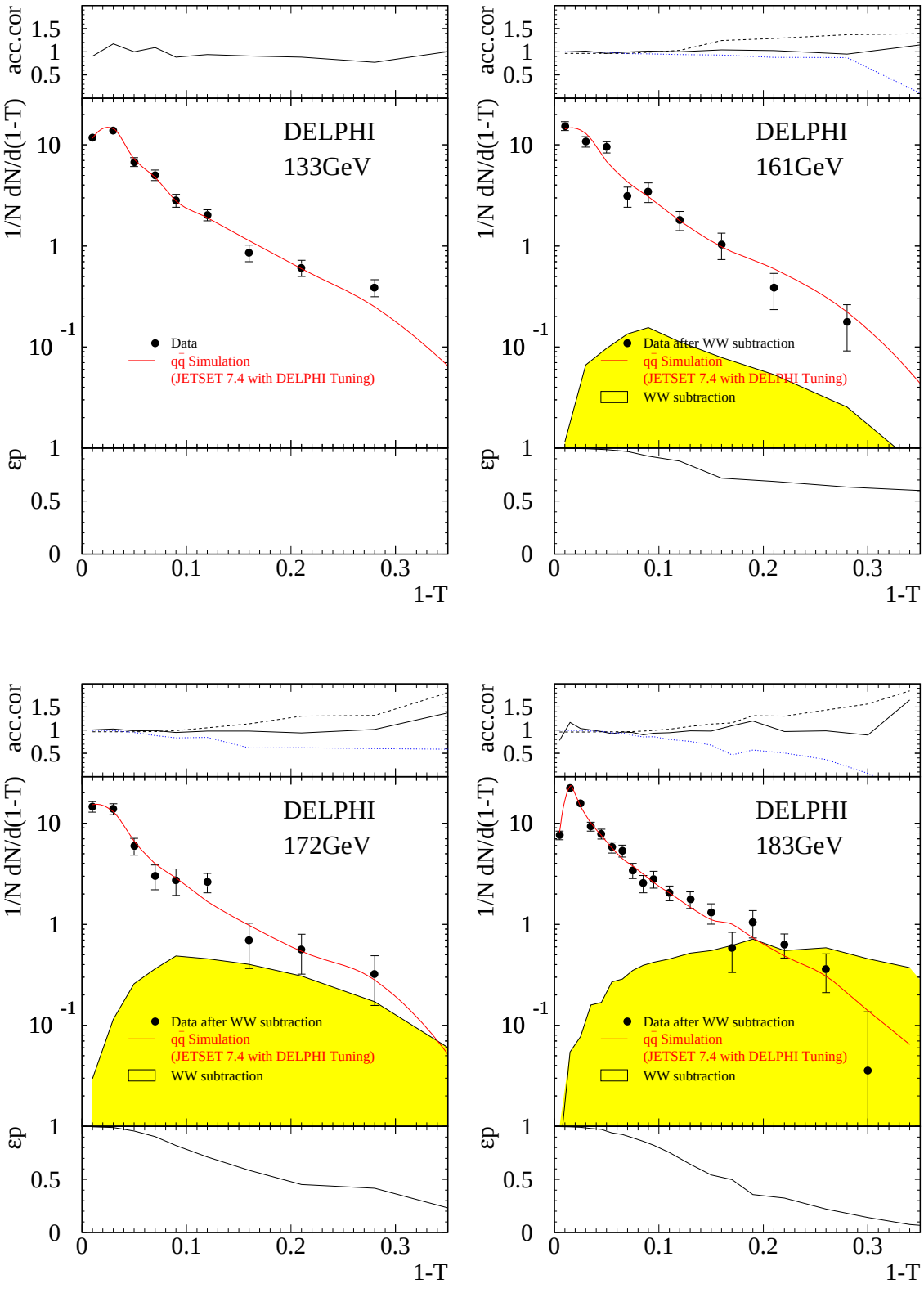


Figure 4: Energy dependence of Thrust distribution. The upper inset shows acceptance corrections: the QCD corrections C_{QCD} as continuous line, the QCD correction due to WW-cuts C_{WW} as dashed line and the ratio of data before and after WW subtraction as dotted line. The middle part shows data, simulation and WW background. The lower part shows the efficiency times purity of the applied WW-cuts.

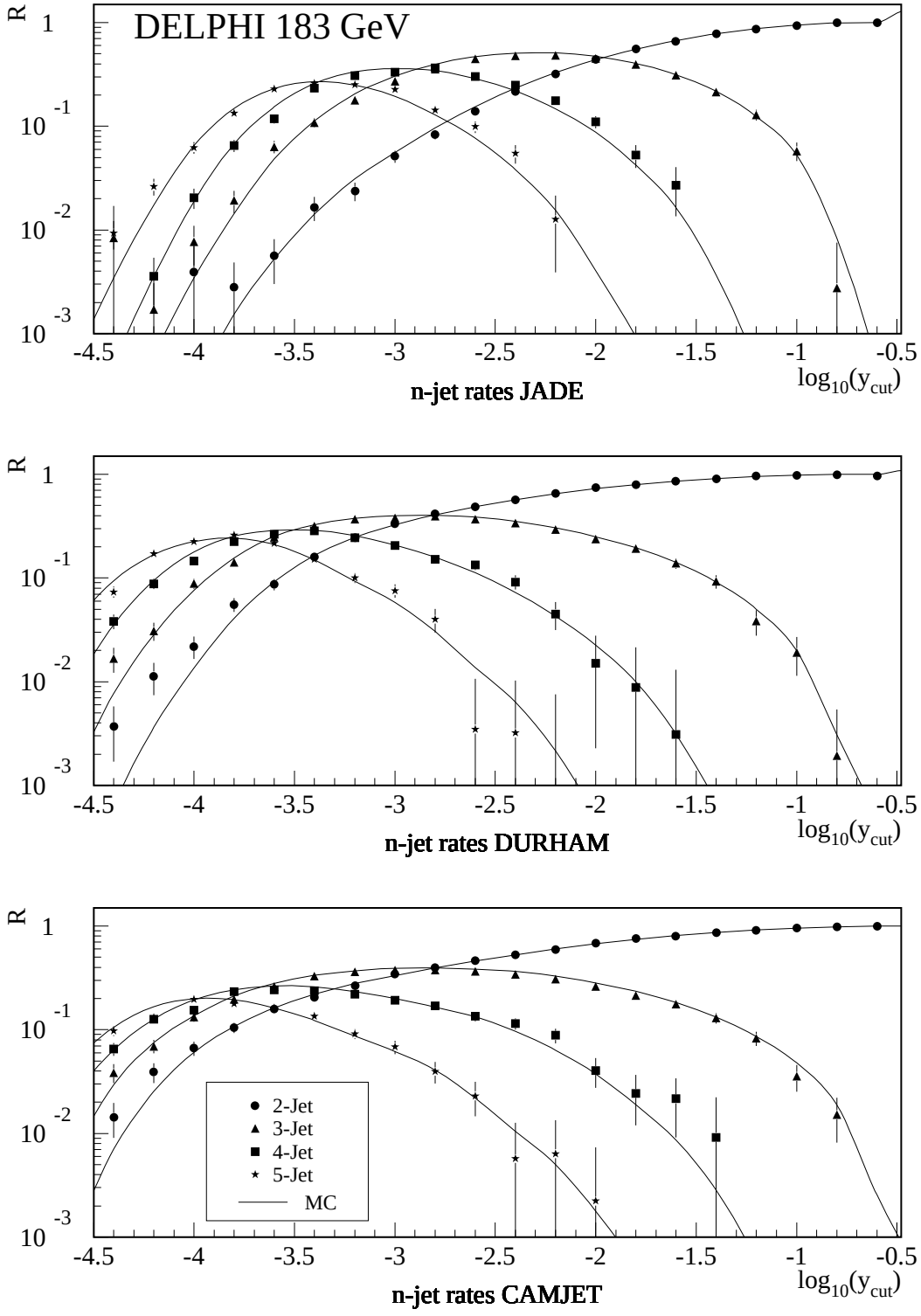


Figure 5: QCD jet rates (R) as a function of y_{cut} compared to the prediction of JETSET7.4 PS

the various systematic error contributions described above, the statistical spread of each systematic uncertainty is investigated. This is done by using multiple sets of full detector simulation with the correct mixing and proper fluctuation of $q\bar{q}$ and WW events, having statistics corresponding to the one of real data. These pseudo data sets are then analysed in the same way as real data, leading to multiple results for each of the systematic error contributions. In case the spread of a contribution is larger than the error found on real data no statement about this error contribution can be made within the given statistics and it set to zero. In case the spread is smaller than the value found on data the spread is quadratically subtracted from this value to get the final systematic error contribution. This method of subtracting the statistical component of systematic errors is applied only to errors obtained by cut variations, and only to the low statistics data ($E_{\rm cm} \geq 133\,\mathrm{GeV}$).

Systematic errors resulting from this procedure are subject to statistical fluctuation since significant contributions are calculated from cut variations. In order to keep the procedure transparent and to keep the fluctuations visible they are not smoothed.

Figure 5 shows the jet rates R_2, R_3, R_4 and R_5 as a function of $y_{\rm cut}$ as determined with the JADE, DURHAM and CAMJET jet algorithms for the 183 GeV data. The CAMJET algorithm is a modified $k_\perp$-clustering jet algorithm similar to the DURHAM algorithm. It preserves the advantages of the original DURHAM algorithm while reducing non-perturbative corrections and providing better resolution of jet substructure. A detailed description of the CAMJET algorithm can be found in [**?**]. Within errors, the data at all energies agree with the generator predictions tuned to Z data. No indication for a significant excess of multi-jet events is observed.

4 Determination of α_s

4.1 α_s from mean event shapes

Event shape means $\langle f \rangle$ are determined using all hadronic events, and thus they have the advantage of minimising the statistical error and are therefore especially well suited for low statistics analyses.

The analytical power ansatz for non-perturbative corrections by Dokshitzer and Webber [**?**,**?**] including the Milan factor established by Dokshitzer et. al. [**?**,**?**] is used to determine α_s from mean event shapes. This ansatz provides an additive term to the perturbative $\mathcal{O}(\alpha_s^2)$ QCD prediction.

$$\langle f \rangle = \frac{1}{\sigma_{\rm tot}} \int f \frac{df}{d\sigma} d\sigma = \langle f_{\rm pert} \rangle + \langle f_{\rm pow} \rangle \tag{2}$$

where the 2nd order perturbative prediction can be written as

$$\langle f_{\rm pert} \rangle = A \frac{\alpha_s(\mu)}{2\pi} + \left(A \cdot 2\pi b_0 \log \frac{\mu^2}{E_{\rm cm}^2} + B \right) \left(\frac{\alpha_s(\mu)}{2\pi} \right)^2, \tag{3}$$

with A and B being known numbers [**?**,**?**], μ being the renormalisation scale and $b_0 = (33 - 2N_f)/12\pi$. The power correction is given by

$$\langle f_{pow} \rangle = c_f \frac{4C_F}{\pi^2} \mathcal{M} \frac{\mu_I}{E_{\rm cm}} \left[\alpha_0(\mu_I) - \alpha_s(\mu) - \left(b_0 \cdot \log \frac{\mu^2}{\mu_I^2} + \frac{K}{2\pi} + 2b_0 \right) \alpha_s^2(\mu) \right] \tag{4}$$

where α_0 is a non-perturbative parameter accounting for the contributions to the event shape below an infrared matching scale μ_I, $K = (67/18 - \pi^2/6)C_A - 5N_f/9$. The Milan

Observable	$\alpha_0(2\,\mathrm{GeV})$	$\alpha_s(M_\mathrm{Z})$	χ^2/ndf
$\langle 1-T\rangle$	$0.493 \pm 0.009 \pm 0.004$	$0.1191 \pm 0.0015 \pm 0.0051$	50.3/26
$\langle M_\mathrm{h}^2/E_\mathrm{vis}^2\rangle$	$0.550 \pm 0.024 \pm 0.013$	$0.1192 \pm 0.0022 \pm 0.0037$	2.65/15

Table 4: Determination of α_0 from a combined fit of α_0 and α_s to a large set of measurments of different experiments [?]. For $E_\mathrm{cm} \geq M_\mathrm{Z}$ only DELPHI measurements are included in the fit. The first error is the statistical error from the fit, the second one is the scale error.

factor $\mathcal{M}$ is set to 1.8, which corresponds to three active flavours in the non-perturbative region. The observable-dependent constant c_f is 2 and 1 for $f = \langle 1-T\rangle$ and $f = \langle M_\mathrm{h}^2/E_\mathrm{vis}^2\rangle$, respectively. The infrared matching scale is set to 2 GeV as suggested by the authors [?], the renormalisation scale μ is set to be equal to E_cm.

Beside α_s these formulae contain α_0 as the only free parameter. In order to measure α_s from individual high energy data this parameter has to be known.

To infer α_0, a combined fit of α_s and α_0 to a large set of measurements at different energies [?] is performed. For $E_\mathrm{cm} \geq M_\mathrm{Z}$ only DELPHI measurements are included in the fit. Figure 6 shows the measured mean values of $\langle 1-T\rangle$ and $\langle M_\mathrm{h}^2/E_\mathrm{vis}^2\rangle$ as a function of the centre of mass energy together with the results of the fit. The resulting values of α_0 are summarised in Table 4. The extracted α_0 values are around 0.5 as expected in [?,?]. However, the numerical values are incompatible with each other. Thus the assumed universality [?] is not valid to the precision that is accessible from the data, though the inclusion of the second order result for $c_{\langle M_\mathrm{h}^2/E_\mathrm{vis}^2\rangle}$ [?,?] reduces the disagreement from about 20% to 10%. Therefore, α_0 is determined for $\langle 1-T\rangle$ and $\langle M_\mathrm{h}^2/E_\mathrm{vis}^2\rangle$ individually. The scale error is obtained by varying the renormalisation scale $x_\mu = \mu^2/E_\mathrm{cm}^2$ from 0.25 to 4.

After having fixed α_0, the α_s values corresponding to the high energy data points can be calculated from Eqs. (2–4). α_s is calculated for both observables individually and then combined with an unweighted average. Its error is propagated from the data and combined by assuming maximal correlation. An additional scale error is calculated by varying x_μ in the ranges discussed and the infrared matching scale μ_I from 1 GeV to 3 GeV. The results are summarised in Table 5 and plotted as function of E_cm together with the QCD expectation in Figure 8.

The α_s values follow the QCD expectation. However, a fit assuming a constant $\alpha_s(E_\mathrm{cm})$ still has a 3% probability. The slope of the logarithmic energy dependence of the inverse strong coupling, α_s^{-1}, is:

$$\frac{\mathrm{d}\alpha_\mathrm{s}^{-1}(\mathrm{E_{cm}})}{\mathrm{d}\log \mathrm{E_{cm}}} = 2b_0\left(1 + \frac{b_1}{b_0^2\log(E_\mathrm{cm}^2/\Lambda^2)} + \ldots\right), \tag{5}$$

with $b_1 = (153 - 19N_f)/24\pi^2$. To first order this quantity is independent of α_s and E_cm. Evaluating Eq. (5) in full second order with $E_\mathrm{cm} = 135\,\mathrm{GeV}$, $\Lambda = 200\,\mathrm{MeV}$ and $N_f = 5$ yields $\mathrm{d}\alpha_\mathrm{s}^{-1}/\mathrm{d}\log \mathrm{E_{cm}} = 1.27$.

A measurement of this slope is obtained by fitting a straight line to the data in the α_s^{-1} vs. $\log E_\mathrm{cm}$ plane. Its systematic error is obtained by raising/lowering the fitted α_s values by their systematic error contribution due to ISR and WW. All other systematics present in the α_s results are considered to be fully correlated, thus not contributing to the

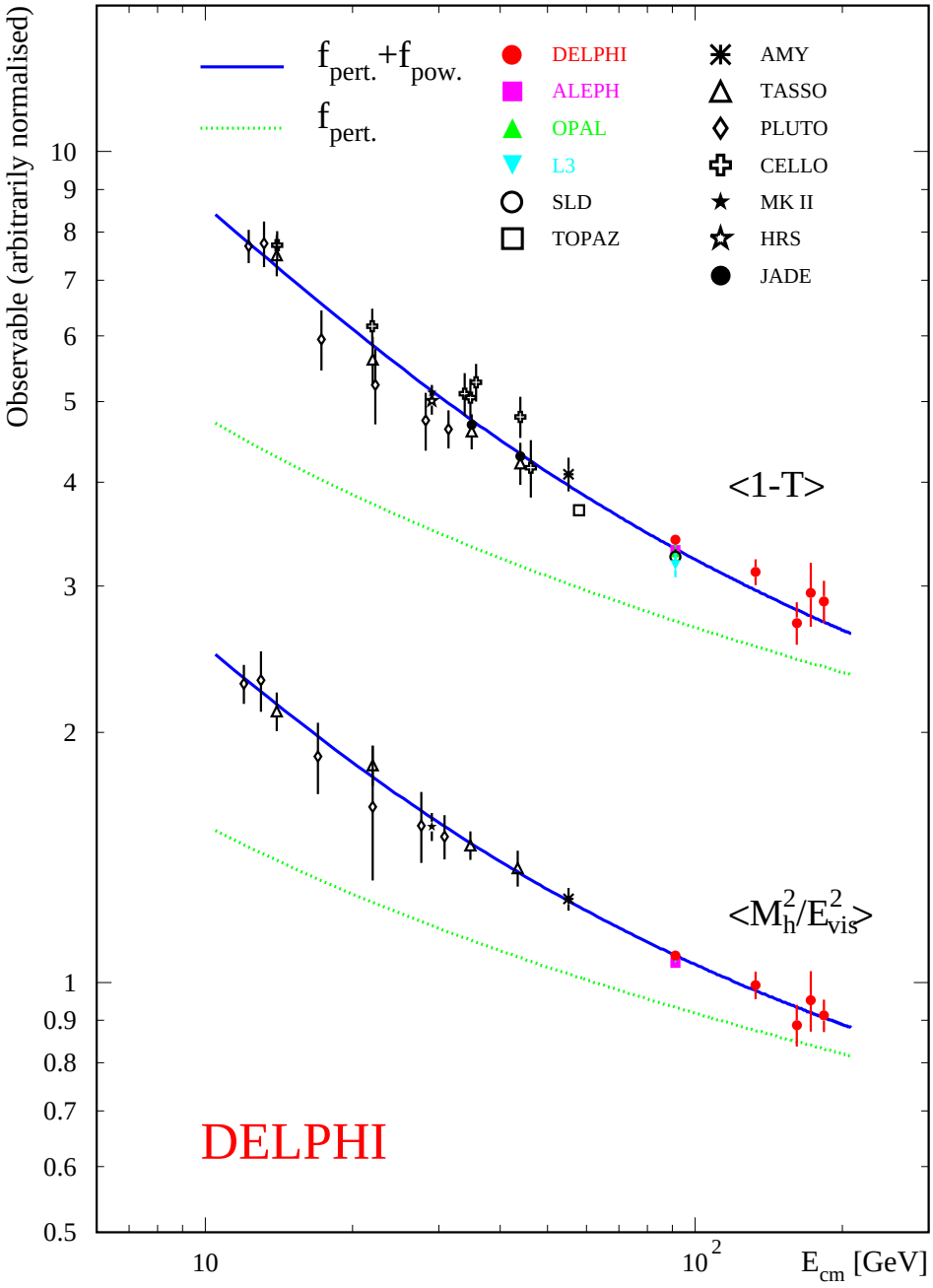


Figure 6: Measured mean values of $\langle 1-T\rangle$ and $\langle M_{\mathrm{h}}^2/E_{\mathrm{vis}}^2\rangle$ as a function of the centre of mass energy. The solid lines present the results of the fits with Eqs. (2–4), the dotted lines show the perturbative part only.

$E_{\rm cm}$	QCD-parameter	Result $\pm$ stat $\pm$ syst $\pm$ scale
91.2 GeV	$\alpha_s(M_{\rm Z})$	$0.1210 \pm 0.0002 \pm 0.0019 \pm 0.0042$
133 GeV	$\alpha_s(133\,{\rm GeV})$	$0.1167 \pm 0.0045 \pm 0.0011 \pm 0.0038$
	$\alpha_s(M_{\rm Z})$	$0.1237 \pm 0.0051 \pm 0.0012 \pm 0.0043$
161 GeV	$\alpha_s(161\,{\rm GeV})$	$0.1048 \pm 0.0063 \pm 0.0053 \pm 0.0031$
	$\alpha_s(M_{\rm Z})$	$0.1134 \pm 0.0075 \pm 0.0062 \pm 0.0036$
172 GeV	$\alpha_s(172\,{\rm GeV})$	$0.1142 \pm 0.0096 \pm 0.0015 \pm 0.0036$
	$\alpha_s(M_{\rm Z})$	$0.1258 \pm 0.0119 \pm 0.0018 \pm 0.0044$
183 GeV	$\alpha_s(183\,{\rm GeV})$	$0.1111 \pm 0.0053 \pm 0.0033 \pm 0.0034$
	$\alpha_s(M_{\rm Z})$	$0.1234 \pm 0.0067 \pm 0.0042 \pm 0.0042$

Table 5: α_s as obtained with the Dokshitzer and Webber ansatz by averaging the $\langle 1-T\rangle$ and $\langle M_{\rm h}^2/E_{\rm vis}^2\rangle$ results.

systematic error of the slope. The result agrees with the QCD expectation of a running α_s (Table 6).

4.2 α_s from Event Shape Distributions

From event shape distributions, α_s is determined by fitting an α_s dependent QCD prediction folded with a hadronisation correction to the data. As QCD predictions $\mathcal{O}(\alpha_s^2)$, pure NLLA, and the combined $\mathcal{O}(\alpha_s^2)$+NLLA in $\ln R$-scheme are employed [?,?,?]. The hadronisation correction is calculated using the JETSET PS model (Version 7.4 as tuned by DELPHI [?]). The QCD prediction is multiplied in each bin by the hadronisation correction

$$C_{\rm had}(E_{\rm cm}) = \frac{f_{\rm had}^{\rm Sim.}(E_{\rm cm})}{f_{\rm part}^{\rm Sim.}(E_{\rm cm})} \quad , \tag{6}$$

where $f_{\rm had}^{\rm Sim.}(E_{\rm cm})$ ($f_{\rm part}^{\rm Sim.}(E_{\rm cm})$) is the model prediction on hadron (parton) level at the centre of mass energy $E_{\rm cm}$. The parton level is defined as the final state of the parton shower created by the simulation.

The fit ranges used for the different QCD predictions are shown in Figure 7. The upper limit of the range used for $\mathcal{O}(\alpha_s^2)$+NLLA is reduced with respect to previous publications [?,?] in order to reduce the systematic uncertainties due to WW background. The lower limit is chosen such that the χ^2/ndf for the QCD fit was reasonable at 183 GeV while maintaining the results at the Z-peak stable. The ranges for pure NLLA and $\mathcal{O}(\alpha_s^2)$ fits are chosen to be distinct, so that the results are statistically uncorrelated. Their limit is taken from [?], where the size of hadronisation correction, the size of the B-coefficient, and the stability under fit range changes is considered.

In [?] it has been shown that fixing the renormalisation scale to $\mu^2 = E_{\rm cm}^2$ results in a marginal description of the data. Therefore, the experimentally optimised scales $x_\mu = \mu^2/E_{\rm cm}^2$ are determined from the LEP1 data and are used for the $\mathcal{O}(\alpha_s^2)$ fits to the high energy data for both observables individually. In contrast for the NLLA and the combined NLLA+$\mathcal{O}(\alpha_s^2)$ fits, μ is set equal to $E_{\rm cm}$, so that these results can be compared to other experiments more directly.

Theory used for measurement	$\mathrm{d}\alpha_\mathrm{s}^{-1}/\mathrm{d}\log(\mathrm{E_{cm}})$
$\mathcal{O}(\alpha_s^2)$+ power ansatz	$1.17 \pm 0.43 \pm 0.18$
$\mathcal{O}(\alpha_s^2)$	$1.14 \pm 0.41 \pm 0.20$
NLLA	$1.69 \pm 0.53 \pm 0.33$
$\mathcal{O}(\alpha_s^2)$+NLLA ($\ln R$-scheme)	$1.39 \pm 0.34 \pm 0.17$
QCD expectation	1.27
QCD+Gluinos expectation	0.90

Table 6: Results of straight line fit to the logarithmic energy dependence of α_s^{-1}, and theoretical expectations calculated in 2nd order.

The systematic errors are obtained from fits to $1-T$ and $M_\mathrm{h}^2/E_\mathrm{vis}^2$ distributions evaluated with different cuts using the same variations as for the error determination of the moments. Again, the resulting systematic errors are reduced by their spread as described in Section 3. The scale errors for the NLLA and $\mathcal{O}(\alpha_s^2)$+NLLA analyses are calculated by varying x_μ from 0.25 to 4. The scale errors for $\mathcal{O}(\alpha_s^2)$ are taken from a previous DELPHI publication [**?**]. An error from the influence of the used hadronisation model is estimated by calculating C_had with JETSET and ARIADNE. The resulting two values of α_s are averaged to get the central value, half of their difference is added in quadrature to the systematic error.

The α_s values evaluated from the distributions are given in Table 8 and plotted in Figure 8. The results agree well with those measured from the event shape means. As for the α_s results from mean event shapes, the data follow the QCD expectation. Fitting a constant α_s yields probabilities of 6% for $\mathcal{O}(\alpha_s^2)$ and below 0.5% for NLLA and $\mathcal{O}(\alpha_s^2)$+NLLA. The slope obtained from fitting a straight line to the logarithmic energy dependence of α_s^{-1} is in good agreement with the QCD expectation (Table 6).

Though one would expect to find light gluinos in direct searches before their influence can be seen in the current measurements of the running of α_s, it is instructive to compare the result to QCD+gluino expectation [**?**] in order to judge the achieved precision. Inverting the first order QCD prediction for the energy dependence of α_s, the measured running corresponds to an observed number of flavours of $N_f = 3.4 \pm 3.2$ ($\mathcal{O}(\alpha_s^2)$+NLLA). The difference between standard QCD and QCD+gluinos thus is at the 1σ-level.

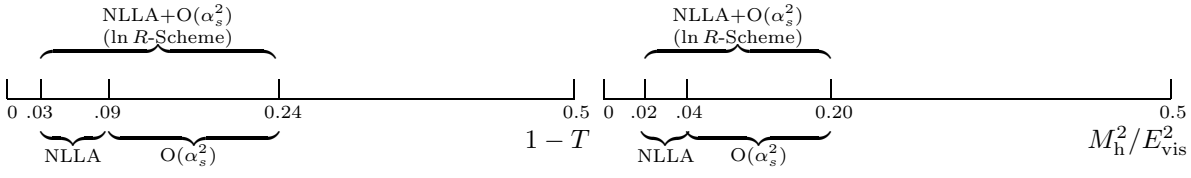


Figure 7: Fit ranges chosen for fitting α_s from different QCD predictions of $1-T$ and $M_\mathrm{h}^2/E_\mathrm{vis}^2$ distribution.

5 Summary

A measurement of event shape distributions and their moments is presented as obtained from data measured at 91.2 GeV, 133 GeV, 161 GeV, 172 GeV and 183 GeV centre of mass energy. Fragmentation models describe the energy evolution of the event shape distributions well. The observed jet rates give no indication for an excess of multi-jet events at high energies.

The strong coupling constant α_s has been determined from the means and the distributions of $1-T$ and $M_{\mathrm{h}}^2/E_{\mathrm{vis}}^2$ using $\mathcal{O}(\alpha_s^2)$, NLLA, and combined QCD predictions (see Table 8 and 5).

Non-perturbative corrections to the shape means were based on their energy evolution using a power correction ansatz. For the shape distributions these non-perturbative corrections were performed using the fragmentation models JETSET and ARIADNE. Within the large statistical errors of the high energy data the different methods yield consistent results.

The comparison of α_s as measured at the Z and at higher energies confirms that the energy dependence (running) of the strong coupling is consistent with QCD expectation. The logarithmic energy slope of the inverse strong coupling is to first order independent of the energy and of α_s. It is measured to be

$$\frac{\mathrm{d}\alpha_{\mathrm{s}}^{-1}}{\mathrm{d}\log(\mathrm{E_{cm}})} = 1.39 \pm 0.34(stat) \pm 0.17(syst) \quad ,$$

in good agreement with the QCD expectation of $1.27 \simeq 2b_0$ (see Eq. (5)).

Acknowledgements

We are greatly indebted to our technical collaborators, to the members of the CERN-SL Division for the excellent performance of the LEP collider, and to the funding agencies for their support in building and operating the DELPHI detector.
We acknowledge in particular the support of
Austrian Federal Ministry of Science and Traffics, GZ 616.364/2-III/2a/98,
FNRS–FWO, Belgium,
FINEP, CNPq, CAPES, FUJB and FAPERJ, Brazil,
Czech Ministry of Industry and Trade, GA CR 202/96/0450 and GA AVCR A1010521,
Danish Natural Research Council,
Commission of the European Communities (DG XII),
Direction des Sciences de la Matière, CEA, France,
Bundesministerium für Bildung, Wissenschaft, Forschung und Technologie, Germany,
General Secretariat for Research and Technology, Greece,
National Science Foundation (NWO) and Foundation for Research on Matter (FOM), The Netherlands,
Norwegian Research Council,
State Committee for Scientific Research, Poland, 2P03B06015, 2P03B03311 and SPUB/P03/178/98,
JNICT–Junta Nacional de Investigação Científica e Tecnológica, Portugal,
Vedecka grantova agentura MS SR, Slovakia, Nr. 95/5195/134,
Ministry of Science and Technology of the Republic of Slovenia,
CICYT, Spain, AEN96–1661 and AEN96-1681,
The Swedish Natural Science Research Council,
Particle Physics and Astronomy Research Council, UK,
Department of Energy, USA, DE–FG02–94ER40817.

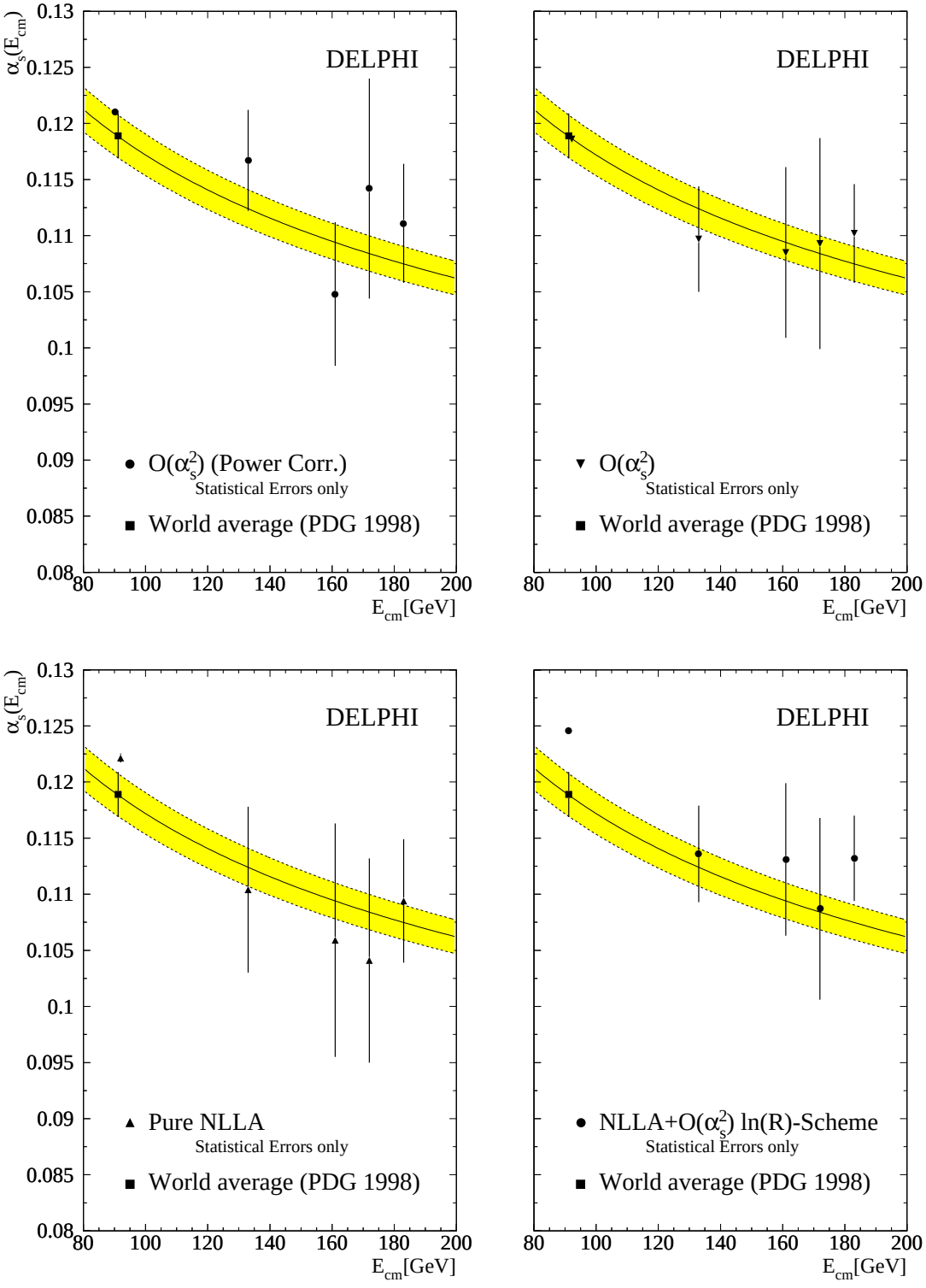


Figure 8: Energy dependence of α_s as obtained from mean event shapes (top left) compared to α_s obtained from distributions. The errors shown are statistical only. The band shows the QCD expectation when extrapolating the world average [**?**] to other energies.

$E_{\rm cm}$	Mean	2nd Moment	3rd Moment
		$1-T$	
91.2 GeV	0.06823 ± 0.00006 ± 0.00065	0.00837 ± 0.00002 ± 0.00009	0.001504 ± 0.000004 ± 0.000016
133 GeV	0.0624 ± 0.0022 ± 0.0005	0.0078 ± 0.0006 ± 0.0001	0.00144 ± 0.00015 ± 0.00003
161 GeV	0.0542 ± 0.0032 ± 0.0025	0.0058 ± 0.0008 ± 0.0003	0.00092 ± 0.00019 ± 0.00005
172 GeV	0.0588 ± 0.0052 ± 0.0011	0.0071 ± 0.0015 ± 0.0005	0.00124 ± 0.00046 ± 0.00020
183 GeV	0.0575 ± 0.0033 ± 0.0016	0.0068 ± 0.0011 ± 0.0004	0.00118 ± 0.00038 ± 0.00011
		$< B_{\rm max} >$	
91.2 GeV	0.07442 ± 0.00005 ± 0.00038	0.00782 ± 0.00001 ± 0.00006	0.001069 ± 0.000002 ± 0.000008
133 GeV	0.0699 ± 0.0018 ± 0.0008	0.0075 ± 0.0004 ± 0.0002	0.00108 ± 0.00009 ± 0.00003
161 GeV	0.0664 ± 0.0026 ± 0.0019	0.0064 ± 0.0005 ± 0.0003	0.00082 ± 0.00010 ± 0.00003
172 GeV	0.0695 ± 0.0038 ± 0.0010	0.0075 ± 0.0009 ± 0.0002	0.00109 ± 0.00018 ± 0.00003
183 GeV	0.0675 ± 0.0020 ± 0.0017	0.0070 ± 0.0005 ± 0.0003	0.00095 ± 0.00010 ± 0.00006
		$< M_{\rm h}^2/E_{\rm vis}^2 >$	
91.2 GeV	0.05383 ± 0.00005 ± 0.00073	0.00524 ± 0.00001 ± 0.00007	0.000761 ± 0.000002 ± 0.000007
133 GeV	0.0496 ± 0.0019 ± 0.0004	0.0053 ± 0.0005 ± 0.0001	0.00087 ± 0.00012 ± 0.00003
161 GeV	0.0444 ± 0.0026 ± 0.0026	0.0040 ± 0.0005 ± 0.0004	0.00056 ± 0.00013 ± 0.00014
172 GeV	0.0476 ± 0.0040 ± 0.0006	0.0050 ± 0.0009 ± 0.0002	0.00080 ± 0.00023 ± 0.00002
183 GeV	0.0456 ± 0.0020 ± 0.0017	0.0043 ± 0.0005 ± 0.0004	0.00063 ± 0.00011 ± 0.00011
		$< y_{32}^{k_\perp} >$	
91.2 GeV	0.02090 ± 0.00004 ± 0.00020	0.00197 ± 0.00001 ± 0.00004	0.000305 ± 0.000002 ± 0.000009
133 GeV	0.0220 ± 0.0018 ± 0.0002	0.0025 ± 0.0004 ± 0.0001	0.00046 ± 0.00012 ± 0.00002
161 GeV	0.0184 ± 0.0031 ± 0.0013	0.0020 ± 0.0009 ± 0.0004	0.00042 ± 0.00025 ± 0.00011
172 GeV	0.0225 ± 0.0040 ± 0.0019	0.0028 ± 0.0010 ± 0.0008	0.00057 ± 0.00028 ± 0.00024
183 GeV	0.0187 ± 0.0019 ± 0.0010	0.0016 ± 0.0004 ± 0.0002	0.00024 ± 0.00011 ± 0.00003

Table 7: Event shape means and higher moments. The first error is statistical, the second systematic. Systematic errors shown in this table are subject to statistical fluctuation since significant contributions are calculated from cut variations. In order to keep the procedure transparent and to keep the fluctuations visible they are not smoothed.

$E_{\rm cm}$	Theory	QCD-parameter	Result $\pm$ stat $\pm$ sys $\pm$ scale
91.2 GeV	$\mathcal{O}(\alpha_s^2)$	$\alpha_s(M_{\rm Z})$	$0.1186 \pm 0.0002 \pm 0.0015 \pm 0.006$
	NLLA	$\alpha_s(M_{\rm Z})$	$0.1221 \pm 0.0002 \pm 0.0039 \pm 0.0087$
	$\mathcal{O}(\alpha_s^2)$+NLLA	$\alpha_s(M_{\rm Z})$	$0.1246 \pm 0.0002 \pm 0.0024 \pm 0.0063$
133 GeV	$\mathcal{O}(\alpha_s^2)$	$\alpha_s(133\,{\rm GeV})$	$0.1097 \pm 0.0046 \pm 0.0009 \pm 0.005$
		$\alpha_s(M_{\rm Z})$	$0.1158 \pm 0.0052 \pm 0.0010 \pm 0.006$
	NLLA	$\alpha_s(133\,{\rm GeV})$	$0.1104 \pm 0.0074 \pm 0.0020 \pm 0.0057$
		$\alpha_s(M_{\rm Z})$	$0.1166 \pm 0.0082 \pm 0.0023 \pm 0.0064$
	$\mathcal{O}(\alpha_s^2)$+NLLA	$\alpha_s(133\,{\rm GeV})$	$0.1136 \pm 0.0043 \pm 0.0013 \pm 0.0048$
	($\ln R$-scheme)	$\alpha_s(M_{\rm Z})$	$0.1202 \pm 0.0048 \pm 0.0014 \pm 0.0053$
161 GeV	$\mathcal{O}(\alpha_s^2)$	$\alpha_s(161\,{\rm GeV})$	$0.1085 \pm 0.0076 \pm 0.0011 \pm 0.005$
		$\alpha_s(M_{\rm Z})$	$0.1178 \pm 0.0091 \pm 0.0012 \pm 0.006$
	NLLA	$\alpha_s(161\,{\rm GeV})$	$0.1059 \pm 0.0104 \pm 0.0015 \pm 0.0046$
		$\alpha_s(M_{\rm Z})$	$0.1147 \pm 0.0123 \pm 0.0018 \pm 0.0054$
	$\mathcal{O}(\alpha_s^2)$+NLLA	$\alpha_s(161\,{\rm GeV})$	$0.1131 \pm 0.0068 \pm 0.0021 \pm 0.0046$
	($\ln R$-scheme)	$\alpha_s(M_{\rm Z})$	$0.1232 \pm 0.0080 \pm 0.0026 \pm 0.0055$
172 GeV	$\mathcal{O}(\alpha_s^2)$	$\alpha_s(172\,{\rm GeV})$	$0.1093 \pm 0.0094 \pm 0.0010 \pm 0.005$
		$\alpha_s(M_{\rm Z})$	$0.1199 \pm 0.0113 \pm 0.0012 \pm 0.006$
	NLLA	$\alpha_s(172\,{\rm GeV})$	$0.1041 \pm 0.0091 \pm 0.0011 \pm 0.0057$
		$\alpha_s(M_{\rm Z})$	$0.1139 \pm 0.0107 \pm 0.0013 \pm 0.0070$
	$\mathcal{O}(\alpha_s^2)$+NLLA	$\alpha_s(172\,{\rm GeV})$	$0.1087 \pm 0.0081 \pm 0.0013 \pm 0.0042$
	($\ln R$-scheme)	$\alpha_s(M_{\rm Z})$	$0.1193 \pm 0.0098 \pm 0.0016 \pm 0.0050$
183 GeV	$\mathcal{O}(\alpha_s^2)$	$\alpha_s(183\,{\rm GeV})$	$0.1102 \pm 0.0044 \pm 0.0019 \pm 0.005$
		$\alpha_s(M_{\rm Z})$	$0.1222 \pm 0.0054 \pm 0.0023 \pm 0.006$
	NLLA	$\alpha_s(183\,{\rm GeV})$	$0.1094 \pm 0.0055 \pm 0.0028 \pm 0.0056$
		$\alpha_s(M_{\rm Z})$	$0.1212 \pm 0.0068 \pm 0.0034 \pm 0.0070$
	$\mathcal{O}(\alpha_s^2)$+NLLA	$\alpha_s(183\,{\rm GeV})$	$0.1132 \pm 0.0038 \pm 0.0013 \pm 0.0049$
	($\ln R$-scheme)	$\alpha_s(M_{\rm Z})$	$0.1259 \pm 0.0048 \pm 0.0016 \pm 0.0061$

Table 8: α_s as obtained from distributions by avaraging the results from the $1-T$ and $M_{\rm h}^2/E_{\rm vis}^2$. The scale errors for the $\mathcal{O}(\alpha_s^2)$ analyses are taken from a previous DELPHI publication [**?**].